Highly Active and Stable CH$_4$ Oxidation by Substitution of Ce^{4+} by Two Pd^{2+} Ions in CeO$_2$(111)

Ya-Qiong Su, Jin-Xun Liu, Ivo A. W. Filot, Long Zhang, and Emiel J. M. Hensen*

Laboratory of Inorganic Materials Chemistry, Schuit Institute of Catalysis, Eindhoven University of Technology, P.O. Box 513, 5600 MB Eindhoven, The Netherlands

S *Supporting Information*

ABSTRACT: Methane (CH$_4$) combustion is an increasingly important reaction for environmental protection, for which Pd/CeO$_2$ has emerged as the preferred catalyst. There is a lack of understanding of the nature of the active site in these catalysts. Here, we use density functional theory to understand the role of doping of Pd in the ceria surface for generating sites highly active toward the C−H bonds in CH$_4$. Specifically, we demonstrate that two Pd^{2+} ions can substitute one Ce^{4+} ion, resulting in a very stable structure containing a highly coordinated unsaturated Pd cation that can strongly adsorb CH$_4$ and dissociate the first C−H bond with a low energy barrier. An important aspect of the high activity of the stabilized isolated Pd cation is its ability to form a strong σ-complex with CH$_4$, which leads to effective activation of CH$_4$. We show that also other transition metals like Pt, Rh, and Ni can give rise to similar structures with high activity toward C−H bond dissociation. These insights provide us with a novel structural view of solid solutions of transition metals such as Pt, Pd, Ni, and Rh in CeO$_2$, known to exhibit high activity in CH$_4$ combustion.

KEYWORDS: CH$_4$ activation, Pd-doped CeO$_2$, solid solutions, density functional theory, mechanism, DFT+U
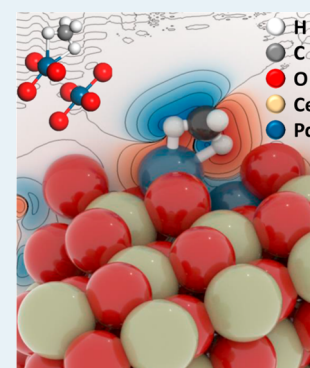
INTRODUCTION

Methane (CH$_4$) is a significant greenhouse gas with a global warming potential ca. 20 times higher than that of CO$_2$.[1] Accordingly, it is desirable to develop technologies to remove residual CH$_4$ present from the exhaust of increasingly popular natural gas engines.[2−6] The challenge is to develop highly active catalysts that can operate at the relatively low temperatures of the exhaust gas. The high Pd loading in the current generation of preferred Pd/CeO$_2$ catalysts poses a cost challenge, requiring a deeper understanding of the nature of the active sites.[1,7−9] In automotive three-way catalysis, Pd is already extensively used to catalyze hydrocarbon oxidation.[10−13] The function of CeO$_2$ in these catalysts is mainly to store and release oxygen, while more recently its ability to maintain a high dispersion of transition metals has been emphasized.[14−16] Although the importance of a close interaction between Pd and CeO$_2$ in catalytic oxidation chemistry has been clearly demonstrated,[1,3,7,17] the exact structure of the active Pd species remains unclear. It has for instance been shown that isolated PdO$_x$ species on the surface of CeO$_2$ are crucial for the low-temperature CO oxidation performance in Pd/CeO$_2$.[18]

Several studies mention the importance of bulk PdO for high CH$_4$ combustion activity.[1,3,7,11,19] Computational studies support this by showing that the (101) surface termination of PdO contains under-coordinated Pd atoms able to form a strong σ-adsorption complex with CH$_4$.[11,19−22] Conventionally, CH$_4$ dissociation on metal surfaces relies on high CH$_4$ translational energies to enhance the sticking probability. In the context of low-temperature CH$_4$ activation, a Langmuir−

Hinshelwood mechanism for CH$_4$ combustion is preferred. A recent study of Weaver and co-workers also showed that CH$_4$ adsorbs strongly on under-coordinated Ir atoms in the IrO$_2$(110) surface, resulting in low-temperature C−H bond activation.[23]

However, the activity of PdO alone is not sufficient to explain the Pd-CeO$_2$ synergy observed for CH$_4$ activation. Cargnello et al. showed that PdO species at the Pd−ceria interface account for the high CH$_4$ combustion activity, while PdO reduction into metallic Pd at $T > 850\ °C$ is causing deactivation.[1] Trovarelli and co-workers proposed that highly dispersed Pd, specifically Pd in a PdO$_4$ square-planar coordination environment, is the most likely active site for CH$_4$ oxidation.[3] Lu and co-workers showed that removal of PdO nanoparticles from a PdO/Ce$_{1−x}$Pd$_x$O$_{2-\sigma}$ catalyst significantly improves CH$_4$ oxidation, emphasizing the important role of a solid solution of Pd in CeO$_2$.[7] The relevance of such solid solutions in ceria-based catalysis is increasingly recognized.[24−27] Recent literature also suggests that solid ceria solutions of Pt, Pd, Ni, and Rh may be crucial to explain CH$_4$ combustion at low temperature.[7,17,28−30]

Usually, doping of transition metals in ceria is modeled by replacing a surface cerium atom by a transition metal atom. For Pd-doped CeO$_2$(111), we recently considered a conventional octahedral configuration as well as a novel and more stable square-planar configuration for CH$_4$ oxidation.[27] The

predicted CH_4 dissociation rates on these models were lower than on $PdO(101)$ due to weak CH_4 adsorption.[24,27] Earlier, Janik and co-workers considered models in which more than one Pd atom are embedded in the ceria lattice and which can lead to facile CH_4 activation in combination with PdO clusters.[26,31] We emphasize that these models including the thermodynamically stable (111)-$3Pd^{2+}$ configuration also cannot explain the experimentally observed high CH_4 oxidation activity of Pd-CeO_2 solid solutions. Janik and co-workers proposed that the $Pd^{2+} \leftrightarrow Pd^{4+}$ transitions contribute to the high activity of Pd-CeO_2 solid solution.[26,31] However, structures containing Pd^{4+} (e.g., (111)-$1Pd^{4+}/2Pd^{2+}$) are thermodynamically unstable under reaction conditions. Thermodynamically stable models will only contain Pd^{2+},[27] in agreement with experimental XPS and XRD data on Pd-CeO_2 solid solution.[3,32−34]

An important corollary of previous data for single-Pd-atom modified CeO_2 surfaces is that CH_4 bonding is extremely weak, i.e., only physical adsorption occurs.[24,27] Accordingly, adsorbed CH_4 is not effectively activated by Pd^{2+} in these configurations. As a result, the computed energy barriers for CH_4 dissociation are higher than 0.9 eV and the dissociative adsorption of CH_4 is endothermic.[27] Thus, from a computational point of view models considered hitherto cannot explain the high catalytic activity of transition metal doped CeO_2.[24−27,31,35] In the present work, we show for the first time that one Ce ion is substituted by two Pd ions, resulting in a very thermodynamically stable configuration which is not only sinter-stable but also very reactive toward the C−H bonds in CH_4. One of the Pd ions is 3-fold coordinated by lattice O atoms, while the other is 4-fold coordinated by lattice O atoms. The coordinative unsaturation of this Pd atom results in strong CH_4 chemisorption and activation. We will demonstrate the broader applicability of this concept by computing stability and reactivity of other transition-metal-doped CeO_2 surfaces. These insights are in good agreement with available experimental data.

■ COMPUTATIONAL DETAILS

Density Functional Theory (DFT) Calculations. We carried out spin-polarized calculations within the DFT framework as implemented in the Vienna Ab initio Simulation Package (VASP).[36] The ion−electron interactions were represented by the projector-augmented wave (PAW) method[37] and the electron exchange-correlation by the generalized gradient approximation (GGA) with the Perdew−Burke−Ernzerhof (PBE) exchange-correlation functional.[38] The Kohn−Sham valence states were expanded in a plane-wave basis set with a cutoff energy of 400 eV. The $Ce(5s,5p,6s,4f,5d)$, $O(2s,2p)$, $Pd(4d5s)$, and $C(2s,2p)$ electrons were treated as valence states. We have used the DFT+U approach, in which U is a Hubbard-like term describing the on-site Coulombic interactions.[39] This approach improves the description of localized states in ceria, where standard LDA and GGA functionals fail. For Ce, a value of $U = 4.5$ eV was adopted, which was calculated self-consistently by Fabris et al.[40] using the linear response approach of Cococcioni and de Gironcoli[41] and which is within the 3.0−6.0 eV range that provides localization of the electrons left upon oxygen removal from ceria.[42] For the calculations of TM-doped $CeO_2(111)$ (TM = transition metal = Pd, Pt, Ni, Rh, Cu and Zn), we used a periodic slab with a (4×4) supercell in which one of the surface Ce atoms was substituted by one TM atom. The

$CeO_2(111)$ slab model is three Ce−O−Ce layers thick and the vacuum gap was set to 15 Å. The atoms in the bottom layer were frozen to their bulk position and only the top two Ce−O−Ce layers were allowed to relax. The bulk lattice constant (5.49 Å) as previously calculated using the PBE+U ($U = 4.5$ eV) functional was used.[43] For the Brillouin zone integration, a Monkhorst−Pack $1 \times 1 \times 1$ mesh was used. To examine the influence of the size of the Monkhorst−Pack grid, we computed the CH_4 adsorption energy on a Pd_1/Pd-dop-II model at Monkhorst−Pack $1 \times 1 \times 1$ and $2 \times 2 \times 2$ meshes. Both the absolute and CH_4 adsorption energies are the same for both mesh sizes. Accordingly, we computed all energies in the Γ-point. The climbing image nudged-elastic band (CI-NEB) algorithm[44,45] was used to identify the transition states for the CH_4 activation and dissociation on selected models.

Microkinetic Model. The dissociation of CH_4 from a molecularly adsorbed precursor state was described by the following kinetic scheme[23,46]

$$CH_4 + * \underset{k_{des}}{\overset{k_{ads}}{\rightleftarrows}} CH_4*$$

$$CH_4* + [O] \overset{k_r}{\rightarrow} CH_3* + H - [O]$$
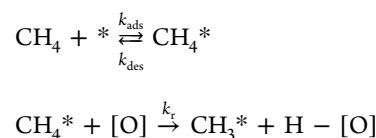
Here, [O] is a lattice oxygen atom neighboring a Pd atom. To compute the reaction rate of CH_4 dissociation, we follow a Langmuir−Hinshelwood type kinetic model,[47] in which we assume that the C−H bond dissociation step is slower than the adsorption/desorption steps of CH_4 (i.e., adsorption of CH_4 is quasi-equilibrated). CH_4 dissociation is usually considered to be irreversible. The equilibrium constant K for molecular CH_4 adsorption is given by

$$K = \frac{k_{ads}}{k_{des}} = \frac{\theta_{CH_4}}{\theta_* P_{CH_4}} \tag{1}$$

in which k_{ads} and k_{des} are the adsorption and desorption rate constants, P_{CH_4} is the methane partial pressure and θ_{CH_4} and θ_* are the coverage with CH_4 and the fraction of empty sites, respectively. The site balance leads to the following expression for the coverage of molecularly adsorbed CH_4

$$\theta_{CH_4} = \frac{KP_{CH_4}}{1 + KP_{CH_4}} \tag{2}$$

The equilibrium constant can be written as

$$K = e^{-\Delta G(T,P)/k_B T} = e^{-[E_{ads} - \mu(T,P)]/k_B T} \tag{3}$$

where $\Delta G(T,P)$, E_{ads}, and $\mu(T,P)$ are the Gibbs free energy change due to molecular CH_4 adsorption, the DFT-computed adsorption energy of molecularly adsorbed CH_4 and the chemical potential of gaseous CH_4 at the temperature T and pressure P, respectively. The chemical potential of methane was given as below

$$\mu(T, P) = \mu(T, P^\theta) + RT \ln\left(\frac{P_{CH_4}}{P^\theta}\right)$$

$$= [H(T, P^\theta) - H(0K, P^\theta)] - T[S(T, P^\theta) - S(0K, P^\theta)]$$

$$+ RT \ln\left(\frac{P_{CH_4}}{P^\theta}\right) \tag{4}$$

where P^θ is the standard atmospheric pressure, and the enthalpy H and entropy S of methane were obtained from standard thermodynamic tables.[48]

The rate for CH_4 dissociation can then be written as

$$r = k_r \theta_{CH_4} = \frac{k_r K P_{CH_4}}{1 + K P_{CH_4}} \quad (5)$$

in which the rate constant k_r is computed from the computed activation barrier for C−H bond dissociation in adsorbed CH_4 according to

$$k_r = \frac{k_B T}{h} e^{-E_a / k_B T} \quad (6)$$

■ RESULTS AND DISCUSSION

Focusing first on Pd, its substitution for Ce in the CeO_2 surface is energetically favorable and lowers the energy to remove an oxygen surface atom, which creates an oxygen vacancy (V_O).[26,27] While most theoretical studies assume an octahedral Pd coordination arising from the Pd for Ce substitution (retaining the initial octahedral coordination of Ce^{4+} in the surface), we demonstrated that a stable structure exists with nearly the same energy in which Pd adopts a square-planar configuration.[27] This structure is much more active in CO oxidation than the octahedral structure. The conventional octahedral (Pd-dop-I) and the alternative square-planar (Pd-dop-II) models for Pd-doped CeO_2 are shown in Figure 1a.
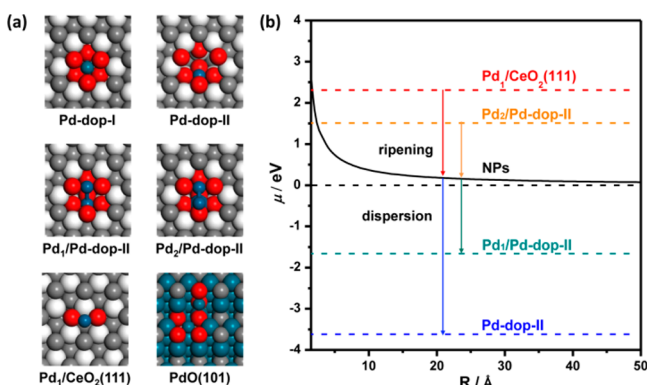

Figure 1. (a) Optimized configurations of Pd atoms dispersed on $CeO_2(111)$. (color code: white = Ce; gray = O; red = O neighboring Pd; cyan = Pd); (b) chemical potential μ of Pd atoms dispersed on $CeO_2(111)$ (dashed lines) and Pd NPs on $CeO_2(111)$ as a function of the nanoparticle radius R (full line). The chemical potential of bulk Pd is set to zero: $\mu_{bulk} = 0$.

CH_4 adsorption is however weak on these Pd-doped surfaces, resulting in a low rate of C−H bond dissociation,[27] orders of magnitude lower than experimentally observed rates.[7] Given the importance of under-coordinated surface atoms in PdO, we should also consider atomically dispersed Pd atoms on the $CeO_2(111)$ surface ($Pd_1/CeO_2(111)$ in Figure 1a) as candidate active sites. However, a previous computational

study showed that these isolated Pd atoms on $CeO_2(111)$ will easily agglomerate into larger clusters via Ostwald ripening.[49] Therefore, we explored an alternative structure in which we added a Pd atom to the single Pd-doped CeO_2.

Figure 1a also shows the surface obtained by adding a Pd atom to the Pd-dop-II surface model (denoted as Pd_1/Pd-dop-II). Adding a Pd atom is favorable ($\Delta E = -1.66$ eV) with respect to bulk Pd, which indicates that the surface Pd atom is very stable in this position. This is further confirmed by the much higher diffusion barrier to an adjacent CeO_2 surface site of 3.37 eV (Figure S2) in comparison to the value of 0.14 eV for Pd_1/CeO_2.[49] When we add a Pd atom to the Pd-dop-I model, the resulting structure spontaneously relaxed to $Pd_1/$Pd-dop-II during geometry optimization in Figure S3. Adding another Pd atom to $Pd_1/$Pd-dop-II is unfavorable ($\Delta E = +1.51$ eV with respect to bulk Pd). Figure 1b shows the chemical potential of the different models in comparison to the chemical potential of supported Pd metal clusters as a function of their size.[50] While $Pd_1/CeO_2(111)$ and $Pd_2/$Pd-dop-II are less stable compared to ceria-supported Pd clusters, Pd-dop-II and $Pd_1/$Pd-dop-II are favored over supported Pd clusters and bulk Pd. $Pd_1/$Pd-dop-II is also stable with respect to the O stoichiometry under typical reaction conditions. The removal of surface O atoms bound to the 3-fold and 4-fold Pd atoms from this structure costs 2.48 and 2.72 eV, respectively. Thus, the O atoms are more strongly bound to the Pd atoms than the O atoms in the stoichiometric CeO_2 surface.[51] It is also important to mention that adsorption of an O atom on the coordinatively unsaturated Pd atom of $Pd_1/$Pd-dop-II is very weak (-0.10 eV). Taken together, these results imply that $Pd_1/$Pd-dop-II is the thermodynamically expected structure under typical oxidative reaction conditions. In essence, the structure is the result of the substitution of one Ce^{4+} ion by two Pd^{2+} ions, which is in line with the much larger radius of Ce^{4+} (0.97 Å) compared to Pd^{2+} (0.64 Å).[33,52−54] The ionic radii are shown in Table 1, while Figure 2 highlights the
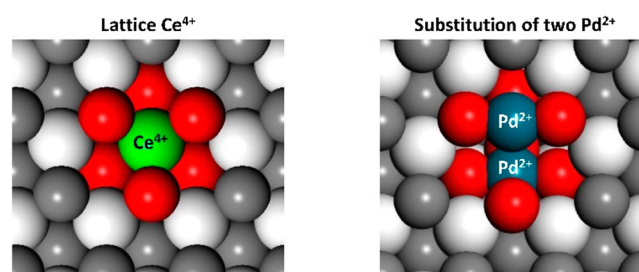

Figure 2. Illustration of the replacement of (left) one lattice Ce^{4+} ion by (right) two Pd^{2+} ions (ionic radii of Ce^{4+} and Pd^{2+} used).

possibility to replace a Ce^{4+} ion by two Pd^{2+} ions. Table 1 also shows that other transition metals can lead to similar structure and this topic will be discussed below. For the Pd case, one of the Pd atoms is coordinated by four lattice O atoms, while the other one is coordinated by three O atoms. We emphasize that this structure is very different from earlier proposed doping models.[24−27,31,35] The unusual aspect of the novel model is

Table 1. Ionic Radii of Various Metal Ions

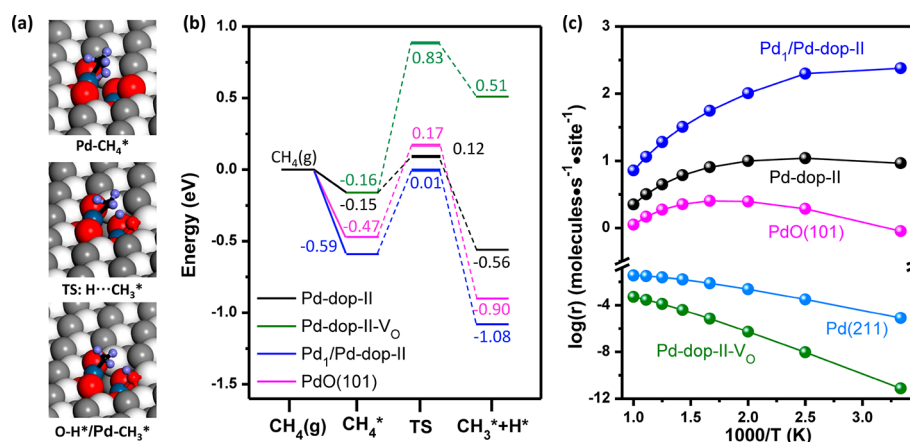| metal	cerium		nickel		palladium		platinum		rhodium			copper		zinc
ion	Ce^{3+}	Ce^{4+}	Ni^{2+}	Ni^{4+}	Pd^{2+}	Pd^{4+}	Pt^{2+}	Pt^{4+}	Rh^{2+}	Rh^{3+}	Rh^{4+}	Cu^+	Cu^{2+}	Zn^{2+}
R (Å)	1.04	0.97	0.69	0.48	0.64	0.63	0.80	0.62	0.72	0.67	0.615	0.46	0.62	0.74

Figure 3. (a) Initial, transition, and final states of CH_4 dissociation by the Pd_1/Pd-dop-II structure; (b) energy profiles of CH_4 adsorption and dissociation by various Pd-containing models; (c) computed CH_4 dissociation rates (T = 300−1000 K, P_{CH_4} = 0.1 atm).

that, unlike earlier models, it contains a stable three-coordinated Pd ion, which we expect to strongly adsorb CH_4. Therefore, we explored in the following the adsorption and activation of CH_4 on the Pd_1/Pd-dop-II structure.

CH_4 adsorption and dissociation are the crucial steps in the CH_4 combustion process.[23,55] The adsorption energy of CH_4 on the Pd_1/Pd-dop-II model is −0.59 eV, which is slightly higher than the value of −0.47 eV computed for the $PdO(101)$ surface. CH_4 adsorbs only weakly on Pd-dop-II. The adsorption energy of −0.15 eV is nearly similar to the adsorption energy on the stoichiometric CeO_2 surface.[27] From this difference, we infer that the presence of a coordinated unsaturated Pd^{2+} ion leads to stronger adsorption. Figure 3a shows the initial adsorption structure of CH_4 as well as the transition and final states for its dissociation into CH_3 and H, resulting in Pd-CH_3 and OH fragments. The potential energy surfaces for CH_4 adsorption and dissociation of CH_4 on this and other models are depicted in Figure 3b. The activation barrier for CH_4 dissociation on Pd_1/Pd-dop-II is 0.60 eV. The adsorption energies of CH_4 on most other models are significantly lower than for Pd_1/Pd-dop-II with comparable or higher barriers (e.g., 0.64 eV for $PdO(101)$ and 0.70 eV for $Pd_1/CeO_2(111)$). The exception is Pd-dop-II, on which CH_4 can be activated with an energy barrier of only 0.27 eV. As discussed before, the low barrier is due to the high activity of the surface O radical.[27] The Pd-dop-II structure is however not stable, and the reactive O atom is spontaneously removed to form the thermodynamically much more stable Pd-dop−II-V_O structure. The activation energy of CH_4 dissociation on this stable surface is 0.99 eV.[27]

In order to compare C−H bond dissociation for the different surface models, we considered a Langmuir−Hinshelwood kinetic scheme in which gaseous CH_4 is quasi-equilibrated with adsorbed CH_4, followed by the slow C−H bond dissociation step, resulting in Pd-CH_3 (CH_3*) and O−H ($H*$) species.[23] This kinetic model together with the computed DFT-energetics predicts that CH_4 dissociation proceeds with the highest rate on Pd_1/Pd-dop-II and then decreases in the order Pd-dop-II > $PdO(101)$ > $Pd(211)$ > Pd-dop-II-V_O (Figure 3c). Although the activation barrier for the C−H bond dissociation on Pd-dop-II is the lowest among the models investigated, the weak adsorption of CH_4 results in a very low CH_4 coverage and, henceforth, a low overall reaction

rate. The thermodynamically preferred structure Pd-dop-II-V_O has the lowest overall reaction rate.

We compare these data to the work of Janik's group on Pd/CeO_2 for CH_4 activation, who studied doping of ceria with multiple Pd atoms.[26,31] Considering only Pd-doping of ceria, a higher activity than $PdO(101)$ is only predicted for their (111)-$1Pd^{4+}/2Pd^{2+}$ structure.[26] However, according to their ab initio phase diagram this structure is not stable under relevant reaction conditions, while the most stable (111)-$3Pd^{2+}$ structure exhibits a more than 2 orders of magnitude lower activity than $PdO(101)$. We also note that the C−H bond distance in the transition states for CH_4 dissociation presented by Janik and co-workers is longer than 2 Å. This distance is too long to represent a C−H bond as one would expect to exist in the transition state for C−H bond dissociation of CH_4. For instance, the C−H distance in the transition states of CH_4 dissociation shown in Figure 3a is around 1.4 Å, close to values reported in the literature.[22,23,27,30] Detailed configurations and the potential energy surface for CH_4 dissociation on Pd_1/Pd-dop-II are shown in Figure S6. Janik and co-workers also investigated PdO clusters supported on Pd-doped ceria.[31] The computed reactivity of these models for CH_4 dissociation are much lower than that of $PdO(101)$.[31] Thus, we can firmly conclude that our proposed model composed of two Pd^{2+} ions in the $CeO_2(111)$ surface as a model for a solid Pd-CeO_2 solution can provide a good explanation for the experimentally observed high CH_4 dissociation activity after removal of PdO from a catalyst containing PdO clusters on a Pd-CeO_2 solid solution.[7] In essence, the coordinatively unsaturated Pd cation in Pd_1/Pd-dop-II is highly reactive toward methane's C−H bonds due to the formation of a strong σ-complex similar to the complex proposed for CH_4 adsorption on $IrO_2(110)$.[23]

We compared in more detail the (electronic) structure of CH_4 adsorbed on Pd_1/Pd-dop-II and $PdO(101)$. In both surfaces, the Pd cation is 3-fold coordinated (Figure 4). Charge analysis shows that CH_4 adsorption on Pd_1/Pd-dop-II leads to an increase of the Pd cation charge, while the reverse holds for the Pd cation in $PdO(101)$ (Table S3). The latter is in line with an earlier computational study.[11] Electron density difference plots before and after CH_4 adsorption on the two surfaces in Figure 4 show that there is a redistribution of electron density between CH_4 and the surface. Moreover, there is clear evidence for the formation of a σ-complex in Pd_1/Pd-dop-II. A density-of-state analysis indicates that 4d-electrons
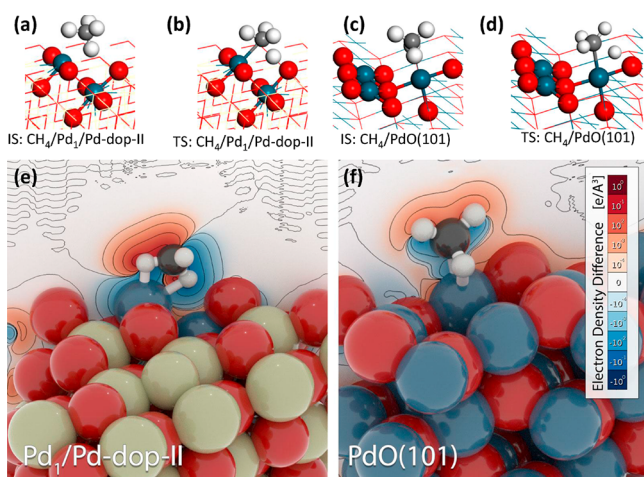
Figure 4. (a,b) Adsorption and transition states of CH_4 by Pd_1/Pd-dop-II. (c,d) Adsorption and transition states of CH_4 by PdO(101). (e,f) Electron density difference contours of CH_4 adsorption on Pd_1/Pd-dop-II and PdO(101). (Color code: cyan = Pd; red = O; off-white = Ce; gray = C; white = H).

from the Pd surface cation in Pd_1/Pd-dop-II effectively overlap with the $1t_2$ frontier molecular orbitals of CH_4 and henceforth strengthen the adsorption of CH_4 (Figure S8). This type of interaction is absent in the CH_4 adsorption complex with PdO(101). Figure 4 also shows that the local coordination environment around CH_4 adsorbed on Pd_1/Pd-dop-II is more favorable for the formation of an O−H bond during C−H bond cleavage. Notably, the C−H bond that will finally dissociate is elongated more in the CH_4 adsorption complex with Pd_1/Pd-dop-II (1.13 Å) than in the corresponding complex with PdO(101) (1.09 Å). This result is important as it shows that a Pd cation at the interface with Pd-doped CeO_2 can strongly adsorb and activate CH_4.

We investigated the feasibility of complete CH_4 oxidation on the Pd_1/Pd-dop-II model. Figure 5 shows the potential energy diagram for the complete catalytic cycle. After CH_4

dissociation, the resulting CH_3* species can be further dehydrogenated to Pd-CH_2 (CH_2*) species and another O−H species (Int2 → Int3). This process is endothermic by 0.55 eV and requires overcoming an activation barrier of 1.05 eV. The CH_2 species on the 3-fold Pd atom will migrate to a neighboring lattice O atom to form a CH_2O species ($\Delta E = -1.79$ eV) with a barrier of only 0.48 eV. Next, an O_2 molecule will adsorb on the 3-fold Pd atom (Int4 → Int5, $E_{ads} = -0.86$ eV). The reaction then further proceeds via a sequence of facile H-transfer steps on the surface forming OOH species that are involved in C−H bond dissociation and H_2O formation. The third C−H bond dissociation step in CH_2O is highly exothermic ($\Delta E = -3.09$ eV). After H_2O desorption (Int7 → Int8), rotation of OCHO occurs, enabling further O_2 adsorption (Int9 → Int10), C−H bond cleavage and formation of CO_2. CO_2 desorption costs 0.52 eV, leaving one oxygen vacancy (Int11 → Int12). Dissociation of OOH heals this vacancy (Int12 → Int13), while the other OH fragment reacts with the remaining H atom to form another H_2O molecule (Int13 → Int14). H_2O desorption ($\Delta E = +1.55$ eV) completes the catalytic cycle.

Overall, the reaction pathway for complete CH_4 oxidation for the novel Pd_1/Pd-dop-II model appears to be feasible. Weaver and co-workers reported that the formation of the CH_2 intermediate is the most difficult step ($E_a = 1.44$ eV) for CH_4 oxidation on PdO(101).[21] The highest barrier for our model is significantly lower ($E_a = 1.05$ eV). Taking into account entropy, we computed that the rate of this C−H bond activation step at 623 K is still 2 orders of magnitude higher than the overall process of adsorption and dissociation of CH_4. The reaction energy diagram also emphasizes the influence of competitive adsorption of O_2 and H_2O. This will shift the operating window of this catalyst to a temperature regime where vacant Pd sites are available. We can compare the O_2 and H_2O adsorption energies of, respectively, −0.82 and −1.55 eV to those for PdO(101), i.e. −1.58 and −1.01 eV, respectively. Thus, while O_2 inhibition is alleviated in our model with respect to PdO(101), competition with H_2O is
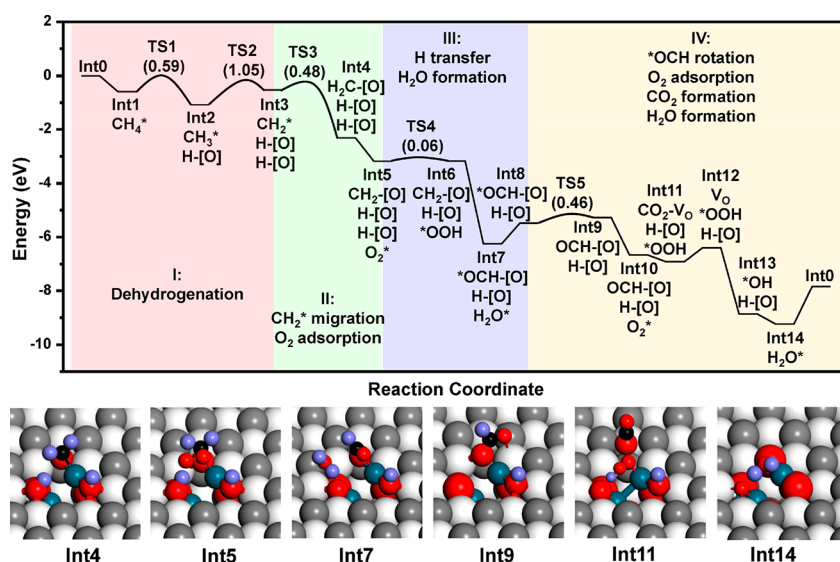

Figure 5. Energy diagram for the reaction $CH_4(g) + 2\,O_2(g) \rightarrow CO_2(g) + 2\,H_2O(g)$ on Pd_1/Pd-dop-II. The structure of selected intermediates (Int) are depicted (all structures in the Supporting Information). The active site * is the 3-fold Pd atom of Pd_1/Pd-dop-II; [O] represents a surface lattice O atom involved in the reaction; V_O represents the oxygen vacancy. (color code: white = Ce; gray = O; red = lattice O neighboring Pd or O of molecular O_2, H_2O or CO_2; cyan = Pd; blue = H).

Table 2. Insertion Energy of the First TM Atom into One Lattice Ce Position Atom (E_{ads}-TM1) and the Second TM Atom (E_{ads}-TM2) with Respect to Corresponding TM Bulk Atoms[a]

TM$_1$/TM-dop-II	Ni	Pd	Pt	Cu	Rh	Zn
E_{ads} (TM1, eV)	−4.79	−3.62	−4.04	−4.20	−4.24	−4.79
E_{ads} (TM2, eV)	−2.03	−1.66	−0.61	−1.22	−1.21	−3.65
E_{ads} (CH$_4$, eV)	−0.42	−0.59	−0.81	−0.41	−0.46	−0.17
E_a (eV)	0.62	0.60	0.49	0.75	0.52	1.10
ΔE (eV)	−0.42	−0.49	−0.77	−0.70	−0.55	0.52
r (molecules·site^{-1}·s^{-1})	1.41×10^{0}	5.57×10^{1}	3.30×10^{4}	9.42×10^{-2}	2.12×10^{1}	1.04×10^{-6}

[a]Adsorption energy E_{ads}, activation energy E_a, reaction energy ΔE of CH$_4$ dehydrogenation, and the rate of CH$_4$ dissociation by TM$_1$/TM-dop-II. P_{CH_4} = 0.1 atm, and T = 623 K.

more prominent. Based on the gas phase entropy of H$_2$O, we can predict that the free energy of H$_2$O desorption is lower than the highest barrier at around 500 K. The occurrence of these competitive effects has been experimentally demonstrated by Weaver and co-workers in a TPD study for PdO(101).[56] The systematic study for PdO(101) by Bossche and Gronbeck showed that CH$_4$ oxidation is inhibited by molecular H$_2$O adsorbed on under-coordinated Pd sites at low temperature.[19] Summarizing, Pd$_1$/Pd-dop-II provides a model on which CH$_4$ can be activated in a facile manner and a complete reaction cycle leading to CO$_2$ and H$_2$O is possible.

Encouraged by these insights, we also investigated the effect of modification of CeO$_2$ with Ni, Pt, Rh, Cu, and Zn, because the former three give rise to active CH$_4$ combustion catalysts in solid solutions,[17,29,30] while the latter two are expected to be low active catalysts. The substitution of all of these transition metals in the CeO$_2$(111) surface is favorable against the bulk of the corresponding transition metal (Table 2). Except for Pt, these transition metals adopt the same square-planar configuration as Pd (Figure S11).[27] The most stable configuration for Pt is the octahedral one, which is likely related to the larger size of Pt in comparison with the other substituents (Table S2). Placement of another like transition metal atom on the doped site is also exothermic, showing the generality of the stabilization of transition metal atoms on doped CeO$_2$. Next, we investigated CH$_4$ adsorption on these structures. The adsorption energy is highest on Pt$_1$/Pt-dop and decreases in the order Pt$_1$/Pt-dop > Pd$_1$/Pd-dop > Rh$_1$/Rh-dop > Ni$_1$/Ni-dop ≈ Cu$_1$/Cu-dop > Zn$_1$/Zn-dop. The electron density difference plots for CH$_4$ adsorbed on Pt$_1$/Pt-dop and Zn$_1$/Zn-dop in Figure S13 show an effective σ-complex formation for the Pt case similar to Pd, while it is absent for Zn. The activation barrier for C−H bond dissociation follows roughly the reverse trend with Zn$_1$/Zn-dop having the highest activation barrier and Pt$_1$/Pt-dop the lowest.

Using the kinetic model for CH$_4$ adsorption and dissociation, we found that the computed rates decreases in the order Pt$_1$/Pt-dop ≫ Pd$_1$/Pd-dop > Rh$_1$/Rh-dop > Ni$_1$/Ni-dop > Cu$_1$/Cu-dop > Zn$_1$/Zn-dop in Figure 6a. At a temperature of 623 K and a CH$_4$ pressure of 0.1 atm, the dissociation rate is higher for the Pt-doped structure than the Pd-doped one. Figure 6b emphasizes the strong correlation between the activation barrier and the distance between the surface and CH$_4$ in the adsorbed state. The decreasing activity at high temperature is because the free energy for desorption is higher than the activation barrier for CH$_4$ dissociation. The free energy change for CH$_4$ adsorption is given by $\Delta E_{ads} - T\Delta S_{ads}$, in which ΔE_{ads} and $T\Delta S_{ads}$ represent the enthalpy and entropy contributions. The activation free energy barrier is
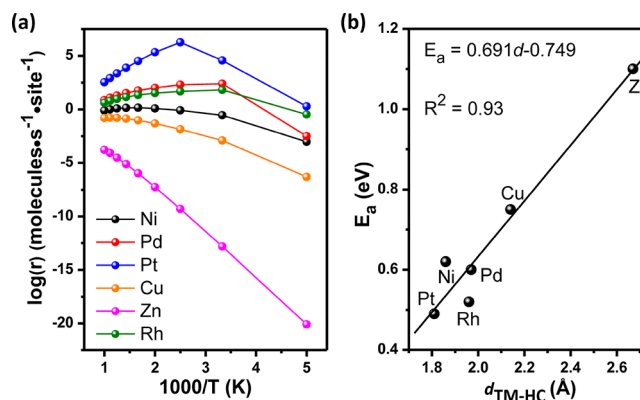

Figure 6. (a) Computed CH$_4$ dissociation rates for various TM$_1$/TM-dop-II structures as a function of temperature with P_{CH_4} = 0.1 atm and (b) relation between CH$_4$ dissociation barrier and the distance between the reactive TM atom and the H atom of the activated C−H bond in CH$_4$ in the adsorbed state.

roughly equal to the activation barrier, as the entropy change during CH$_4$ dissociation starting from the σ-complex is negligible in comparison with the entropy change during adsorption or desorption. The predicted high activity computed for Pt$_1$/Pt-dop-II provides a good explanation for the experimentally reported high activity of a Ce$_{1-x}$Pt$_x$O$_{2-\sigma}$ solid solution.[28,57] In a similar manner, Ni- and Rh-promoted CeO$_2$ catalysts have also been noted for their promising activity in CH$_4$ combustion.[58−62]

■ CONCLUSIONS

We investigated a novel structure of a solid solution of Pd in CeO$_2$ with the purpose of explaining the high activity of Pd-CeO$_2$ solid solutions toward CH$_4$ activation. We show that two Pd^{2+} ions can substitute one Ce^{4+} ion in the stable CeO$_2$(111) surface, resulting in a structure that is stable under oxidative conditions. CH$_4$ will strongly adsorb as a σ-complex on the Pd cation that is coordinatively unsaturated. The CH$_4$ adsorption energy is higher on this novel structure than on PdO(101). Consequently, the activation barrier for dissociation of the adsorbed CH$_4$ molecule is lower for Pd$_1$/Pd-dop-II. Kinetic simulations show that CH$_4$ dissociation proceeds with the highest rate on this structure. We also show that similar structures can be obtained by doping the CeO$_2$(111) surface with Pt, Ni, Rh, Cu, and Zn. Specifically, the more reactive transition metals Pt, Ni, and Rh can lead to strong CH$_4$ adsorption complexes, low C−H activation barriers, and a high CH$_4$ dissociation activity. The concept of substituting two transition metal ions for one Ce^{4+} ion in ceria is important as it results in a very stable structure containing a highly reactive

coordinatively unsaturated transition metal. We expect that this insight opens up new possibilities to rationally design active and stable catalysts of surface doped oxides.

■ ASSOCIATED CONTENT

ⓢ Supporting Information

The Supporting Information is available free of charge on the ACS Publications website at DOI: 10.1021/acscatal.8b01477.

(1) Chemical potential calculations; (2) ab initio thermodynamic analysis, additional structural information, electron density difference analysis, and simulated STM; and (3) complete catalytic cycle of CH_4 oxidation and the configurations of relevant intermediates (PDF)

■ AUTHOR INFORMATION

Corresponding Author

*E-mail: e.j.m.hensen@tue.nl.

ORCID ⓞ

Jin-Xun Liu: 0000-0002-7499-4197
Ivo A. W. Filot: 0000-0003-1403-8379
Emiel J. M. Hensen: 0000-0002-9754-2417

Notes

The authors declare no competing financial interest.

■ ACKNOWLEDGMENTS

■ REFERENCES

(1) Cargnello, M.; Jaén, J. D.; Garrido, J. H.; Bakhmutsky, K.; Montini, T.; Gámez, J. C.; Gorte, R.; Fornasiero, P. Exceptional Activity for Methane Combustion over Modular Pd@CeO₂ Subunits on Functionalized Al₂O₃. *Science* **2012**, *337*, 713−717.

(2) Taifan, W.; Baltrusaitis, J. CH₄ Conversion to Value Added Products: Potential, Limitations and Extensions of a Single Step Heterogeneous Catalysis. *Appl. Catal., B* **2016**, *198*, 525−547.

(3) Colussi, S.; Gayen, A.; Farnesi Camellone, M.; Boaro, M.; Llorca, J.; Fabris, S.; Trovarelli, A. Nanofaceted Pd_O Sites in Pd_Ce Surface Superstructures: Enhanced Activity in Catalytic Combustion of Methane. *Angew. Chem., Int. Ed.* **2009**, *48*, 8481−8484.

(4) Gélin, P.; Primet, M. Complete Oxidation of Methane at Low Temperature over Noble Metal Based Catalysts: a Review. *Appl. Catal., B* **2002**, *39*, 1−37.

(5) Hu, Z.; Li, B.; Sun, X.; Metiu, H. Chemistry of Doped Oxides: the Activation of Surface Oxygen and the Chemical Compensation Effect. *J. Phys. Chem. C* **2011**, *115*, 3065−3074.

(6) Shin, T. H.; Ida, S.; Ishihara, T. Doped CeO₂−LaFeO₃ Composite Oxide as an Active Anode for Direct Hydrocarbon-type Solid Oxide Fuel Cells. *J. Am. Chem. Soc.* **2011**, *133*, 19399−19407.

(7) Meng, L.; Lin, J. J.; Pu, Z. Y.; Luo, L.-F.; Jia, A.-P.; Huang, W. X.; Luo, M. F.; Lu, J. Q. Identification of Active Sites for CO and CH₄ Oxidation over PdO/Ce₁₋ₓPdxO₂₋δ Catalysts. *Appl. Catal., B* **2012**, *119*, 117−122.

(8) Colussi, S.; Trovarelli, A.; Vesselli, E.; Baraldi, A.; Comelli, G.; Groppi, G.; Llorca, J. Structure and Morphology of Pd/Al₂O₃ and Pd/CeO₂/Al₂O₃ Combustion Catalysts in Pd−PdO TransformationHysteresis. *Appl. Catal., A* **2010**, *390*, 1−10.

(9) Hoffmann, M.; Kreft, S.; Georgi, G.; Fulda, G.; Pohl, M.-M.; Seeburg, D.; Berger-Karin, C.; Kondratenko, E. V.; Wohlrab, S. Improved Catalytic Methane Combustion of Pd/CeO₂ Catalysts via Porous Glass Integration. *Appl. Catal., B* **2015**, *179*, 313−320.

(10) Martin, N. M.; Van den Bossche, M.; Hellman, A.; Grönbeck, H.; Hakanoglu, C.; Gustafson, J.; Blomberg, S.; Johansson, N.; Liu, Z.; Axnanda, S.; et al. Intrinsic Ligand Effect Governing the Catalytic Activity of Pd Oxide Thin Films. *ACS Catal.* **2014**, *4*, 3330−3334.

(11) Hellman, A.; Resta, A.; Martin, N.; Gustafson, J.; Trincero, A.; Carlsson, P.-A.; Balmes, O.; Felici, R.; van Rijn, R.; Frenken, J.; et al. The Active Phase of Palladium During Methane Oxidation. *J. Phys. Chem. Lett.* **2012**, *3*, 678−682.

(12) Weaver, J. F. Surface Chemistry of Late Transition Metal Oxides. *Chem. Rev.* **2013**, *113*, 4164−4215.

(13) Weng, X.; Ren, H.; Chen, M.; Wan, H. Effect of Surface Oxygen on the Activation of Methane on Palladium and Platinum Surfaces. *ACS Catal.* **2014**, *4*, 2598−2604.

(14) Zheng, T.; He, J.; Zhao, Y.; Xia, W.; He, J. Precious Metal-Support Interaction in Automotive Exhaust Catalysts. *J. Rare Earths* **2014**, *32*, 97−107.

(15) Jen, H.-W.; Graham, G.; Chun, W.; McCabe, R.; Cuif, J. P.; Deutsch, S.; Touret, O. Characterization of Model Automotive Exhaust Catalysts: Pd on Ceria and Ceria−Zirconia Supports. *Catal. Today* **1999**, *50*, 309−328.

(16) Yao, H.; Yao, Y. Y. Ceria in Automotive Exhaust Catalysts: I. Oxygen Storage. *J. Catal.* **1984**, *86*, 254−265.

(17) Zhu, Y.; Zhang, S.; Shan, J. J.; Nguyen, L.; Zhan, S.; Gu, X.; Tao, F. In Situ Surface Chemistries and Catalytic Performances of Ceria Doped with Palladium, Platinum, and Rhodium in Methane Partial Oxidation for the Production of Syngas. *ACS Catal.* **2013**, *3*, 2627−2639.

(18) Spezzati, G.; Su, Y. Q.; Hofmann, J. P.; Benavidez, A. D.; Delariva, A. T.; McCabe, J.; Datye, A. K.; Hensen, E. J. M. Atomically dispersed Pd-O species on CeO₂(111) as highly active sites for low-temperature CO oxidation. *ACS Catal.* **2017**, *7*, 6887−6891.

(19) Bossche, M. V. d.; Grönbeck, H. Methane Oxidation over PdO(101) Revealed by First-Principles Kinetic Modeling. *J. Am. Chem. Soc.* **2015**, *137*, 12035−12044.

(20) Kinnunen, N. M.; Hirvi, J. T.; Suvanto, M.; Pakkanen, T. A. Role of the Interface Between Pd and PdO in Methane Dissociation. *J. Phys. Chem. C* **2011**, *115*, 19197−19202.

(21) Antony, A.; Asthagiri, A.; Weaver, J. F. Pathways and Kinetics of Methane and Ethane C−H Bond Cleavage on PdO (101). *J. Chem. Phys.* **2013**, *139*, 104702.

(22) Chin, Y. H.; Buda, C.; Neurock, M.; Iglesia, E. Consequences of Metal−Ooxide Interconversion for C−H Bond Activation During CH₄ Reactions on Pd Catalysts. *J. Am. Chem. Soc.* **2013**, *135*, 15425−15442.

(23) Liang, Z.; Li, T.; Kim, M.; Asthagiri, A.; Weaver, J. F. Low-Temperature Activation of Methane on the IrO₂(110) Surface. *Science* **2017**, *356*, 299−303.

(24) Mayernick, A. D.; Janik, M. J. Methane oxidation on Pd−Ceria: A DFT Study of the Mechanism over PdxCe₁₋ₓO₂, Pd, and PdO. *J. Catal.* **2011**, *278*, 16−25.

(25) Mayernick, A. D.; Janik, M. J. Methane Activation and Oxygen Vacancy Formation over CeO₂ and Zr, Pd Substituted CeO₂ Surfaces. *J. Phys. Chem. C* **2008**, *112*, 14955−14964.

(26) Senftle, T. P.; van Duin, A. C.; Janik, M. J. Role of Site Stability in Methane Activation on PdxCe₁₋ₓOδ Surfaces. *ACS Catal.* **2015**, *5*, 6187−6199.

(27) Su, Y. Q.; Filot, I. A. W.; Liu, J. X.; Hensen, E. J. M. Stable Pd-doped Ceria Structures for CH₄ Activation and CO Oxidation. *ACS Catal.* **2018**, *8*, 75−80.

(28) Jin, J.; Li, C.; Tsang, C.-W.; Xu, B.; Liang, C. Catalytic Combustion of Methane over Pt−Ce Oxides under Scarce Oxygen Condition. *Ind. Eng. Chem. Res.* **2016**, *55*, 2293−2301.

(29) Liu, Z.; Grinter, D. C.; Lustemberg, P. G.; Nguyen-Phan, T. D.; Zhou, Y.; Luo, S.; Waluyo, I.; Crumlin, E. J.; Stacchiola, D. J.; Zhou, J.; et al. Dry Reforming of Methane on a Highly-Active Ni-CeO₂ Catalyst: Effects of Metal-Support Interactions on C− H Bond Breaking. *Angew. Chem., Int. Ed.* **2016**, *55*, 7455−7459.

(30) Tang, W.; Hu, Z.; Wang, M.; Stucky, G. D.; Metiu, H.; McFarland, E. W. Methane Complete and Partial Oxidation Catalyzed by Pt-doped CeO₂. *J. Catal.* **2010**, *273*, 125−137.

(31) Senftle, T. P.; van Duin, A. C.; Janik, M. J. Methane Activation at the Pd/CeO₂ Interface. *ACS Catal.* **2017**, *7*, 327−332.

(32) Hiley, C. I.; Fisher, J. M.; Thompsett, D.; Kashtiban, R. J.; Sloan, J.; Walton, R. I. Incorporation of Square-Planar Pd²⁺ in Fluorite CeO₂: Hydrothermal Preparation, Local Structure, Redox Properties and Stability. *J. Mater. Chem. A* **2015**, *3*, 13072−13079.

(33) Gulyaev, R.; Kardash, T. Y.; Malykhin, S.; Stonkus, O.; Ivanova, A.; Boronin, A. The Local Structure of Pd$_x$Ce$_{1-x}$O$_{2-x-\delta}$ Solid Solutions. *Phys. Chem. Chem. Phys.* **2014**, *16*, 13523−13539.

(34) Neitzel, A.; Figueroba, A.; Lykhach, Y.; Skála, T. s.; Vorokhta, M.; Tsud, N.; Mehl, S.; Sevcikova, K.; Prince, K. C.; Neyman, K. M.; et al. Atomically Dispersed Pd, Ni, and Pt Species in Ceria-Based Catalysts: Principal Differences in Stability and Reactivity. *J. Phys. Chem. C* **2016**, *120*, 9852−9862.

(35) Krcha, M. D.; Mayernick, A. D.; Janik, M. J. Periodic Trends of Oxygen Vacancy Formation and C−H Bond Activation over Transition Metal-doped CeO₂(111) Surfaces. *J. Catal.* **2012**, *293*, 103−115.

(36) Kresse, G.; Hafner, J. Ab Initio Molecular-Dynamics Simulation of the Liquid-Metal−Amorphous-Semiconductor Transition in Germanium. *Phys. Rev. B: Condens. Matter Mater. Phys.* **1994**, *49*, 14251.

(37) Blöchl, P. E. Projector Augmented-Wave Method. *Phys. Rev. B: Condens. Matter Mater. Phys.* **1994**, *50*, 17953.

(38) Perdew, J. P.; Burke, K.; Ernzerhof, M. Generalized Gradient Approximation Made Simple. *Phys. Rev. Lett.* **1996**, *77*, 3865.

(39) Dudarev, S.; Botton, G.; Savrasov, S.; Humphreys, C.; Sutton, A. Electron-Energy-Loss Spectra and the Structural Stability of Nickel Oxide: An LSDA+ U Study. *Phys. Rev. B: Condens. Matter Mater. Phys.* **1998**, *57*, 1505.

(40) Fabris, S.; de Gironcoli, S.; Baroni, S.; Vicario, G.; Balducci, G. Reply to "Comment on 'Taming Multiple Valency with Density Functionals: A Case Study of Defective Ceria'. *Phys. Rev. B: Condens. Matter Mater. Phys.* **2005**, *72*, 237102.

(41) Cococcioni, M.; De Gironcoli, S. Linear Response Approach to the Calculation of the EffectiveInteraction Parameters in the LDA+ U Method. *Phys. Rev. B: Condens. Matter Mater. Phys.* **2005**, *71*, 035105.

(42) Castleton, C.; Kullgren, J.; Hermansson, K. Tuning LDA+U for Electron Localization and Structure at Oxygen Vacancies in Ceria. *J. Chem. Phys.* **2007**, *127*, 244704−2447040.

(43) Da Silva, J. L.; Ganduglia-Pirovano, M. V.; Sauer, J.; Bayer, V.; Kresse, G. Hybrid Functionals Applied to Rare-Earth Oxides: The Example of Ceria. *Phys. Rev. B: Condens. Matter Mater. Phys.* **2007**, *75*, 045121.

(44) Henkelman, G.; Jónsson, H. Improved Tangent Estimate in the Nudged Elastic Band Method for Finding Minimum Energy Paths and Saddle Points. *J. Chem. Phys.* **2000**, *113*, 9978−9985.

(45) Sheppard, D.; Terrell, R.; Henkelman, G. Optimization Methods for Finding Minimum Energy Paths. *J. Chem. Phys.* **2008**, *128*, 134106.

(46) Weaver, J. F.; Carlsson, A. F.; Madix, R. J. The Adsorption and Reaction of Low Molecular Weight Alkanes on Metallic Single Crystal Surfaces. *Surf. Sci. Rep.* **2003**, *50*, 107−199.

(47) Liu, J. X.; Su, H. Y.; Sun, D. P.; Zhang, B. Y.; Li, W. X. Crystallographic Dependence of CO Activation on Cobalt Catalysts: HCP versus FCC. *J. Am. Chem. Soc.* **2013**, *135*, 16284−16287.

(48) Stull, D. R.; Prophet, H. *JANAF Thermochemical Tables*; National Standard Reference Data System: Washington, DC, 1971.

(49) Su, Y. Q.; Liu, J. X.; Filot, I. A. W.; Hensen, E. J. M. Theoretical Study of Ripening Mechanisms of Pd Clusters on Ceria. *Chem. Mater.* **2017**, *29*, 9456−9462.

(50) Liu, J. C.; Wang, Y. G.; Li, J. Toward Rational Design of Oxide-Supported Single-Atom Catalysts: Atomic Dispersion of Gold on Ceria. *J. Am. Chem. Soc.* **2017**, *139*, 6190−6199.

(51) Su, Y. Q.; Filot, I. A. W.; Liu, J.-X.; Tranca, I.; Hensen, E. J. M. Charge Transport over the Defective CeO₂(111) Surface. *Chem. Mater.* **2016**, *28*, 5652−5658.

(52) Orera, V.; Merino, R.; Pena, F. Ce³⁺↔ Ce⁴⁺ Conversion in Ceria-Doped Zirconia Single Crystals Induced by Oxido-Reduction Treatments. *Solid State Ionics* **1994**, *72*, 224−231.

(53) Sun, C.; Xue, D. Size-Dependent Oxygen Storage Ability of Nano-sized Ceria. *Phys. Chem. Chem. Phys.* **2013**, *15*, 14414−14419.

(54) Shannon, R. T.; Prewitt, C. T. Effective Ionic Radii in Oxides and Fluorides. *Acta Crystallogr., Sect. B: Struct. Crystallogr. Cryst. Chem.* **1969**, *25*, 925−946.

(55) Zhao, C.; Zhao, Y.; Li, S.; Sun, Y. Effect of Pd Doping on CH₄ Reactivity over Co₃O₄ Catalysts from Density-Functional Theory Calculations. *Chin. J. Catal.* **2017**, *38*, 813−820.

(56) Zhang, F.; Hakanoglu, C.; Hinojosa, J. A., Jr; Weaver, J. F. Inhibition of Methane Adsorption on PdO(101) by Water and Molecular Oxygen. *Surf. Sci.* **2013**, *617*, 249−255.

(57) Mueller, V. H.; Duduković, M. P.; Lo, C. S. The Role of Metal−Support Interaction on Catalytic Methane Activation. *Appl. Catal., A* **2014**, *488*, 138−147.

(58) Lee, M.; Nam, J.; Seo, J. Synthesis of Ni-CeO₂ Catalyst for the Partial Oxidation of Methane using RF Thermal Plasma. *Chin. J. Catal.* **2016**, *37*, 743−749.

(59) Pal, P.; Singha, R. K.; Saha, A.; Bal, R.; Panda, A. B. Defect-Induced Efficient Partial Oxidation of Methane over Nonstoichiometric Ni/CeO₂ Nanocrystals. *J. Phys. Chem. C* **2015**, *119*, 13610−13618.

(60) Duarte, R.; Krumeich, F.; van Bokhoven, J. Structure, Activity, and Stability of Atomically Dispersed Rh in Methane Steam Reforming. *ACS Catal.* **2014**, *4*, 1279−1286.

(61) Yisup, N.; Cao, Y.; Feng, W.-L.; Dai, W.-L.; Fan, K.-N. Catalytic Oxidation of Methane over Novel Ce−Ni−O Mixed Oxide Catalysts Prepared by Oxalate Gel-Coprecipitation. *Catal. Lett.* **2005**, *99*, 207−213.

(62) Boullosa-Eiras, S.; Zhao, T.; Chen, D.; Holmen, A. Effect of the Preparation Methods and Alumina Nanoparticles on the Catalytic Performance of Rh/Zr$_x$Ce$_{1-x}$O$_2$−Al₂O₃ in Methane Partial Oxidation. *Catal. Today* **2011**, *171*, 104−115.